Effect of ultrasound on bone fracture healing

Computers in Biology and Medicine 100 (2018) 74–85

Contents lists available at ScienceDirect

Computers in Biology and Medicine

journal homepage: www.elsevier.com/locate/compbiomed

Effect of ultrasound on bone fracture healing: A computational bioregulatory model

Maria G. Vavva[a], Konstantinos N. Grivas[a], Aurélie Carlier[b,c], Demosthenes Polyzos[a], Liesbet Geris[b,c], Hans Van Oosterwyck[b,c], Dimitrios I. Fotiadis[d,e,*]

[a] Dept. of Mechanical Engineering and Aeronautics, University of Patras, GR 26500, Patras, Greece
[b] Dept. of Mechanical Engineering, KU Leuven, Celestijnenlaan 300C – PB 2419, B-3001, Leuven, Belgium
[c] MERLN Institute for Technology-inspired Regenerative Medicine, Maastricht University, Universiteitssingel 40, 6229 ER, Maastricht, the Netherlands
[d] Dept. of Materials Science and Engineering, University of Ioannina, GR 45110, Ioannina, Greece
[e] Foundation for Research and Technology–Hellas, Institute of Molecular Biology and Biotechnology, Department of Biomedical Research, GR 45110, Ioannina, Greece

ARTICLE INFO

Keywords:
Ultrasound
Bone healing
Angiogenesis
Vascular endothelial growth factor
Computational model

ABSTRACT

Bone healing is a complex biological procedure in which several cellular actions, directed by biochemical and mechanical signals, take place. Experimental studies have shown that ultrasound accelerates bone ossification and has a multiple influence on angiogenesis. In this study a mathematical model predicting bone healing under the presence of ultrasound is demonstrated. The primary objective is to account for the ultrasound effect on angiogenesis and more specifically on the transport of the Vascular Endothelial Growth Factor (VEGF). Partial differential equations describing the spatiotemporal evolution of cells, growth factors, tissues and ultrasound acoustic pressure and velocity equations determining the development of the blood vessel network constitute the present model. The effect of the ultrasound characteristics on angiogenesis and bone healing is investigated by applying different boundary conditions of acoustic pressure at the periosteal region of the bone model, which correspond to different intensity values. The results made clear that ultrasound enhances angiogenesis mechanisms during bone healing. The proposed model could be regarded as a step towards the monitoring of the effect of ultrasound on bone regeneration.

1. Introduction

Fracture healing is a complicated process that includes multiple cellular mechanisms and stages. The process begins with an inflammatory stage, which leads to the creation of the callus and the differentiation of tissues within the callus and is completed with the callus resorption and bone remodeling.

Angiogenesis is a vital part of bone healing, since it re-establishes blood flow at the fracture site, preventing thus ischemic necrosis and allowing repair. Many growth factors, including fibroblast growth factor (FGF), bone morphogenetic protein (BMP), transforming growth factor (TGF), and vascular endothelial growth factor (VEGF) families play a key angiogenic and osteogenic role during fracture healing [4,20]. Although the exact mechanisms behind angiogenesis are not yet fully understood VEGF is known to play a key role [45]. VEGF is produced by cells in hypoxia and diffuses towards existing blood vessels as well as by hypertrophic chondrocytes triggering the endochondral ossification pathway. When VEGF reaches nearby blood vessels it will activate endothelial cells to express “tip cell” phenotype or become “stalk cells”. A tip cell senses microenvironmental stimuli by using filopodia and moves away from its mother vessel giving lead to a new blood vessel branch. The newly developed branches are lengthened through chemotaxis i.e., the movement of the tip cell towards the source of VEGF. As the cell attaches and moves along fibers in the extracellular matrix, there is also a haptotactic component of tip cell motion [46,47].

Several mathematical models and computational studies have been proposed to simulate bone healing in order to elucidate the underlying mechanisms of cell activities and angiogenesis [1,18,22,49]. In 2005 a fuzzy logic model was proposed to model fracture healing [44] and fracture vascularity. In a later study [19] was presented a continuous mathematical model for deriving predictions for bone healing by using a system of partial differential equations in which the unknown variables were the densities of cell types, growth factors and tissues.

* Corresponding author. Address: Unit of Medical Technology and Intelligent Information Systems, Dept. of Materials Science and Engineering, University of Ioannina, GR 45110, Ioannina, Greece.
E-mail addresses: marvavva@gmail.com (M.G. Vavva), konstantinos.grivas@gmail.com (K.N. Grivas), aurelie.carlier@kuleuven.be (A. Carlier), polyzos@mech.upatras.gr (D. Polyzos), liesbet.geris@ulg.ac.be (L. Geris), hans.vanoosterwyck@kuleuven.be (H. Van Oosterwyck), fotiadis@cc.uoi.gr (D.I. Fotiadis).

https://doi.org/10.1016/j.compbiomed.2018.06.024
Received 2 March 2018; Received in revised form 23 June 2018; Accepted 23 June 2018

Angiogenesis process was modeled by employing the spatiotemporal development of endothelial cell concentration and vascular density. The predicted healing process was in accordance with experimental observations. Nevertheless, the authors pointed out that the discrete nature of vasculature couldn't be fully described by continuous variables. To this end the same group extended their work by adapting the system of PDEs so as to describe vascularization with a discrete variable [35]. The proposed angiogenesis model was based on a previous deterministic hybrid model [46], in which a set of PDEs describes the velocity of each tip cell, and also simulated sprout dynamics i.e., blood vessel growth and branching. More recently Carlier et al. [6], refined the model of Peiffer et al. [35], by accounting for an intracellular level in each endothelial cell, which describes the Dll4-Notch signaling pathway. The model could accurately describe bone regeneration process and also capture tip cell selection features that had been previously experimentally observed. This model was further enhanced by explicitly simulating the effect of oxygen on the various cellular mechanisms i.e., differentiation, proliferation, hypoxia signaling and cell death [6]. The authors suggested that such oxygen models could further provide insight to the complicated spatiotemporal interaction of oxygen delivery, diffusion and consumption with the cellular mechanisms during bone healing.

A lattice-based model has also been presented to describe tissue differentiation and angiogenesis in a bone/implant fracture under shear loading [7]. This study was based in the work of Anderson and Caplain [1] in which the tip cell motion was simulated as a probabilistic biased random walk. An additional tissue differentiation stimulus i.e., the oxygen concentration level, was inserted in the mechanoregulatory algorithm in order to account for angiogenesis. Higher loads were found to lead to lower vascularization rates and thus delayed bone formation. The results were in accordance with experimental findings. A similar method was also used in Milde et al. [31], for the determination of the acceleration of tip cells. The role of oxygen availability within callus on cellular mechanisms has been also recently investigated by OReilly et al., [33]. By using computational mechanobiological models with high levels of angiogenic impairment the authors showed that low oxygen levels inhibit chondrocyte hypertrophy and endochondral ossification during tissue regeneration. A rule-based model of sprouting angiogenesis has also been reported in Ref. [39] where the elongation and proliferation of stalk cells as well as the effect of Notch factor production are explicitly simulated.

Ultrasound has been widely used for the investigation of the underlying mechanisms of the ultrasound effect on bone healing process. Physically ultrasound induces mechanical forces at the cellular level, which have been shown to regulate bone formation [32,34]. In an experimental study [9] the authors by applying (Low Intensity Pulsed Ultrasound) LIPUS on osteoporotic fracture rat models found an earlier bridging of the fracture gap and increased amount of callus formation as compared with the control group. In addition, they also found higher amounts of cartilage at weeks 2–4 post-fracture in the LIPUS group suggesting that the earlier callus formation may be attributed to enhanced endochondral ossification. In a more recent review study on the role of ultrasound on osteoporotic bone [8] the authors report that gene expression during the osteoporotic fracture repair has indicated that LIPUS increases callus formation during the early phase, leads to an earlier onset of the remodeling phase and enhances angiogenesis. It was also stated that enhancement effect due to LIPUS application could be partially donated to the local increase of estrogen receptors (ERs) expression in the fracture callus [10].

The acceleration of bone healing course has been widely demonstrated by several clinical [24,27] and animal studies [38] reporting a reduction in healing time by 17–42%. At cellular level, more recent experimental studies have shown that LIPUS enhances cellular mechanisms, such as proliferation and migration, of osteoblasts [52] and osteocytes [16] and also promotes osteogenesis by affecting differentiation of mesenchymal stem and progenitor cells [28].

In a recent experimental study [17] aiming at the investigation of the effect of different LIPUS intensities on fracture healing it was found that low-density bone volume fraction was significantly higher in the group treated with LIPUS Intensity 30 mW/cm^2 than in the control group. LIPUS at higher intensity was found not to further accelerate bone healing. US has also been found to accelerate primary callus formation in femur and fibular osteotomies in rabbits [14]. More specifically it was observed that for the first 10–12 days post-fracture, US caused a rapid increase in callus formation which was then stabilized. On the other hand, this rapid increase in callus formation in control osteotomies occurred at approximately 2 weeks after fracture. In another study [54] by applying US on rat femoral fractures it was found that chondrocytes exhibit a significant increase in aggrecan gene expression after exposure to US, which is correlated with chondrogenesis [25].

Furthermore, ultrasound has been shown to significantly enhance blood vessel formation due to an increase of the levels of cytokines', fibroblast growth factor, and vascular endothelial growth factor (VEGF), which are related to angiogenesis. In two experimental studies of ultrasound application on human osteoblasts, gingival fibroblasts and blood mononuclear cells [13,42] cytokines that are related with angiogenesis were found significantly stimulated in osteoblasts, and VEGF levels were found increased. Increased VGEF expression at week 4–8 post-fracture indicating increased amounts of new blood vessel formation is also reported in Ref. [9]. The authors suggested that angiogenesis is enhanced by LIPUS during the remodeling phase of healing in osteoporotic fractures. In another study [41] it was found that low-intensity power Doppler ultrasound application on ulnar osteotomies in dogs caused increased vascularity in the fracture site which enhances the delivery of growth factors and cytokines necessary for the healing process.

Ultrasound frequency has also been shown to play vital role in angiogenesis. During the inflammatory stage the main US receptors in the granulation tissue are the macrophage [15,29]. In another study of US application on chick chorioallantoic membrane [40] it was also shown that ultrasound can induce angiogenesis *in vivo*. The US effect was more pronounced for specific US intensities and frequencies.

A large number of animal and clinical studies have also investigated the ability of quantitative ultrasound to monitor the healing process [38]. These studies have demonstrated that the propagation velocity across fractured bones can be used as an indicator of healing [38]. Furthermore, the technique of ultrasound axial transmission has been proven effective in providing ultrasonic parameters that are related to long bone's mechanical and geometrical properties.

Researchers have also recently developed computational models of ultrasound wave propagation in bones aiming to further enhance the monitoring capabilities of ultrasound. Nevertheless, these models are currently focused on describing realistic bone geometries and their mechanical properties at a meso- and macro-level [11,32,47]. Furthermore, they primarily aim at investigating the possibility of employing novel means of evaluating the mechanical properties of bone and monitoring the healing course without making any attempt to describe the underlying physiological healing phenomena. On the other hand, mechanobiological and mathematical models have been extensively used to 1) describe the mechanisms by which mechanical loads regulate biological processes through signals to cells and 2) simulate the complex biological processes, such as bone repair which are difficult to be experimentally and clinically studied. Therefore, such models can aid in providing novel insights and fundamental understanding of the influence of US on bone healing.

In this work we present a deterministic hybrid computational model for deriving bone healing and angiogenesis predictions by employing ultrasound stimulation. The model is based on the work of Peiffer et al. [35], consisting of partial differential equations, which describe the spatiotemporal evolution of soft tissues, bone and the development of blood vessel network. For the purposes of the present work, we assume

that ultrasound affects the transport of VEGF by introducing an additional term accounting for the contribution of ultrasound acoustic pressure. An extensive sensitivity analysis for the newly introduced parameters is performed. To account for the influence of the ultrasound characteristics on bone healing predictions, simulations are also conducted for different ultrasound intensities by applying different boundary conditions of acoustic pressure. Since safe conclusions can be drawn only if computational results are interpreted in conjunction with experimental measurements, the proposed model is assessed by comparing the predicted tissue fractions in callus with the corresponding experimental observations provided in Refs. [23,30].

The paper is organized as follows: The new system of partial differential equations governing the fracture healing process under the effect of ultrasound in blood vessel's growth is derived in the next section. The values of the parameters used for model's sensitivity analysis, the initial and boundary conditions as well as the numerical approach adopted in our analysis are illustrated in section 3. The spatiotemporal evolution of tissue fractions and vasculature accompanied with the results of sensitivity analysis are demonstrated and compared with experimental measurements [23,30] in section 4. Finally, the obtained results are analyzed and extensively discussed in sections 5 and 6.

2. The computational multiscale model

In this section the mathematical model utilized in the present computational study is illustrated.

The new ultrasound model builds upon a previously published multiscale model of bone fracture healing and consists of (a) a tissue level describing the various key processes of bone fracture healing with 10 continuous variables and (b) a cellular level representing the developing vasculature with discrete endothelial cells.

The resulting hybrid framework is computationally efficient and suitable to answer the research question at hand, i.e. the investigation of the influence of ultrasound on bone fracture healing. At the cellular level, the development of the discrete vascular tree is determined by sprouting, vascular growth and anastomosis. The growth of a blood vessel is modeled by computing the movement of the corresponding tip cell. Regard that the current model accounts for the effect of ultrasound on the VEGF parameter.

The starting point is the model proposed by Peiffer et al. [35], which includes eleven differential equations describing the spatiotemporal variation of mesenchymal stem cells (c_m), fibroblasts (c_f), chondrocytes (c_c), osteoblasts (c_b), fibrous extracellular matrix (m_f), cartilaginous extracellular matrix (m_c), bone extracellular matrix (m_b), generic osteogenic (g_b), chondrogenic (g_c) and vascular growth factors (g_v), as well as the concentration of oxygen and nutrients (n), i.e.:

$$\frac{\partial c_m}{\partial t} = \nabla\cdot(D_m\nabla c_m - C_{mCT}c_m\nabla(g_b+g_v) - C_{mHT}c_m\nabla m) + A_m c_m(1-\alpha_m c_m) - F_1 c_m - F_2 c_m - F_4 c_m \tag{1}$$

$$\frac{\partial c_f}{\partial t} = \nabla\cdot(D_f\nabla c_f - C_f c_f\nabla g_b) + A_f c_f(1-\alpha_f c_f) + F_4 c_m - F_3 d_f c_f, \tag{2}$$

$$\frac{\partial c_c}{\partial t} = A_c c_c(1-\alpha_c c_c) + F_2 c_m - F_3 c_c \tag{3}$$

$$\frac{\partial c_b}{\partial t} = A_b c_b(1-\alpha_b c_b) + F_1 c_m + F_3 c_c - d_b c_b \tag{4}$$

$$\frac{\partial m_f}{\partial t} = P_{fs}(1-\kappa_f m_f)c_f - Q_f m_f m_c c_b \tag{5}$$

$$\frac{\partial m_c}{\partial t} = P_{cs}(1-\kappa_c m_c)c_c - Q_c m_c c_b \tag{6}$$

$$\frac{\partial m_b}{\partial t} = P_{bs}(1-\kappa_b m_b)c_b \tag{7}$$

$$\frac{\partial g_c}{\partial t} = \nabla\cdot(D_{gc}\nabla g_c) + E_{gc}c_c - d_{gc}g_c \tag{8}$$

$$\frac{\partial g_b}{\partial t} = \nabla\cdot(D_{gb}\nabla g_b) + E_{gb}c_b - d_{gb}g_b \tag{9}$$

$$\frac{\partial g_v}{\partial t} = \nabla\cdot(D_{gv}\nabla g_v) + E_{gvb}c_b + E_{gvc}c_c - g_v(d_{gv}+d_{gvc}c_v) \tag{10}$$

$$\frac{\partial n}{\partial t} = \nabla\cdot(D_n\nabla n) + E_n c_v - d_n n \tag{11}$$

where $m = m_f + m_c + m_b$ is the total tissue density. The processes described by these equations as well as the parameters used in this model are extensively discussed in Geris et al., [19].

Besides, Peiffer et al., [345] propose an angiogenesis description model based on the discrete variable c_v appearing in Eqs. (10) and (11) of the above system and taking the value 1 when a grid volume contains a blood vessel while otherwise $c_v = 0$.

To model the effect of ultrasound we adopt the idea of Xu et al. [53], according to which for a fluid-saturated medium subjected to a small amplitude oscillatory pressure gradient, such as in the case of ultrasound presence, the pressure fluctuation causes micro fluid flow through the sample so that to release the differential pressure. This phenomenon can be described by dynamic diffusion i.e.,

$$\frac{\partial p}{\partial t} = \nabla\cdot(D_p\nabla p) \tag{12}$$

where D_p is the diffusivity of the ultrasound acoustic pressure explained in Xu et al., [53].

Assigning the pressure p to interstitial fluid pressure, pressure gradient is related directly to interstitial fluid velocity through Darcy's law, i.e.

$$\mathbf{u} = -K\nabla p \tag{13}$$

with K being the hydraulic conductivity of the interstitium, also known as permeability coefficient. In case of the absence of US, $\mathbf{u}$ does not exist.

Phipps and Kohandel [37] proposed a mathematical model to describe the diffusion of proangiogenic (f_p) and antiangiogenic (f_a) factors in solid tumors described by the equation

$$\frac{\partial f_j}{\partial t} = D_j\nabla^2 f_j - k_j f_j + g_j - \nabla\cdot(\mathbf{u}f_j), \quad j = p, a \tag{14}$$

with D_j, k_j and g_j illustrated in Phipps and Kohandel [37].

Adopting their idea, Eq. (10) is properly modified so that to introduce the contribution of interstitial fluid velocity to VEGF g_v, i.e.

$$\frac{\partial g_v}{\partial t} = \nabla\cdot(D_{gv}\nabla g_v) + E_{gvb}c_b + E_{gvc}c_c - g_v(d_{gv}+d_{gvc}c_v) - \nabla\cdot(\mathbf{u}g_v) \tag{15}$$

where $\mathbf{u}$ satisfies Eq. (13).

Finally, writing Eq. (15) in terms of interstitial pressure p by replacing $\mathbf{u}$ via Darcy's law (Eq. (13)) we obtain

$$\frac{\partial g_v}{\partial t} = \nabla\cdot(D_{gv}\nabla g_v + Kg_v\nabla p) + E_{gvb}c_b + E_{gvc}c_c - g_v(d_{gv}+d_{gvc}c_v) \tag{16}$$

Equations (1)–(9) and (11) and (12) and (16) constitute the system of PDEs that describes the new model proposed in the present work.

The non-dimensionalized parameters, variables and functional forms related to migration, proliferation, chondrogenic differentiation and growth factor production given in Eqs. (1)–(9) and (11) and (16) are the same as those given in Peiffer et al., [35]. Regarding blood vessel formation when a grid volume of the spatial discretization

contains a vessel, the variable c_v is set to 1, otherwise $c_v = 0$. The evolution of c_v is determined by blood vessel growth, branching and anastomosis, as proposed by Peiffer et al., [35].

Blood vessel growth is modeled by solving tip velocity equations that describe the movement of the corresponding tip cell [35,46]. Branching i.e., new tip creation, occurs for high VEGF concentrations and anastomosis when a tip cell meets a blood vessel i.e., when the tip cell reaches a grid volume i.e., when the tip cell reaches a grid volume with $c_v = 1$.

3. Material properties, geometry and numerical implementation

In the present section a sensitivity analysis on the parameters used in the above described model, the initial and boundary conditions of the bone healing boundary value problem and the numerical methodology employed for the solution of the PDE system are illustrated.

The diffusivity of ultrasound acoustic pressure D_p was derived by using the equation $D_p = k/\varphi\eta\beta$, as reported in Ref. [53], where k, φ, η *and* β are permeability, porosity, viscosity and compressibility factor respectively. At $t = 0$, since bone callus is filled only with granulation tissue, D_p is calculated using the corresponding material properties and equals to 28.7×10^{-3} mm^2/day [12].

Regarding the hydraulic conductivity K as previously mentioned it equals to the permeability coefficient and for granulation tissue equals to $10^{-14} m^4/Ns$ [12]. Nevertheless, in order to investigate the sensitivity of the model outcome to different combinations between D_p and K numerical simulations are also performed for $K = 10^{-15}$ and $K = 10^{-16}$ m$^{4/N}$ which correspond to permeability values reported in the literature for cartilage and bone respectively [12,26].

The effect of ultrasound intensity on bone healing mechanisms for $K = 10^{-14} m^4/Ns$, which was found to be the most optimal case by means of blood vessel growth, is investigated for four different ultrasound intensities i.e., $I_1 = 15$, $I_2 = 25$, $I_3 = 50$ and $I_4 = 75$ mW/cm^2. For a linear plane wave propagation, the intensity is proportional to the square of acoustic pressure:

$$I = \frac{|p|^2}{Z} \tag{17}$$

where p is the acoustic pressure and Z the acoustic impedance.

Equation (17) can be obtained as follows:

$$I = P_o / V = F \times V / A = P \times V = >$$

$$I = P \times V \tag{18}$$

For a plane acoustic wave:

$$P = \rho \times c \times V \tag{19}$$

Combining (18) and (19) one can get:

$$I = P2 / \rho c = > I = P2 / Z$$

where: P_o = Power, A = Area, F = Force, V = Velocity, c = Sound Speed, ρ = density, P = Pressure.

By using the acoustic impedance of blood i.e., $Z = 1.66$ kg/m^2, and the four examined values of I i.e., I_1, I_2, I_3 and I_4, Eq. (17) derives $p_1 = 0.8$, $p_2 = 2$, $p_3 = 4$ and $p_4 = 6.1$ kPa respectively which serve as different boundary conditions applied at the periosteal region of the model as described below.

The model parameters were non-dimensionalized in accordance with Peiffer et al., [35]. Regarding the newly introduced parameters they were non-dimensionalized as follows (tildes refer to non-dimensionalized parameters):

$$\widetilde{D}_p = \frac{D_p T}{L^2}, \widetilde{K} = \frac{KT}{L^4} F_o, \widetilde{p} = \frac{p}{p_0}$$

where $T = 1$ day, $L = 3.5$ mm (a parameter used by Peiffer et al. [35], for non-dimensionalization), $F_0 = 1{,}5$ kN and $p_0 = 1$ kPa. Therefore, the dimensionalized diffusivity of ultrasound acoustic pressure is $\widetilde{D}_p = 2.35 \times 10^{-3}$ and the three examined values of the hydraulic conductivity are $\widetilde{K} = 0.001$, $\widetilde{K} = 0.01$ and $\widetilde{K} = 0.1$.

Numerical calculations were performed on a spatial domain derived from a real callus geometry of a standardized femoral rodent fracture [23]. A real scanning acoustic microscopy (SAM) image, the geometry of the fracture callus, the initial positions of the endothelial cell and the boundary conditions are depicted in Fig. 1 (those are the same as the ones used by Peiffer et al. [35]).

The values of the initial and boundary conditions are based on Gerstenfeld et al., [21]. No-flux boundary conditions are considered for all variables, except for those depicted in Fig. 1. Due to symmetry issues only one-fourth of the domain is considered. Initially the callus is assumed to consist of fibrous tissue i.e., $m_f^{init} = 10$ mg/ml. Mesenchymal stem cells and fibroblasts are also assumed to be released into the callus tissue from the periosteum, the surrounding tissues and the bone marrow ($c_m^{bc} = 2 \times 10^4$ cells/ml and $c_f^{bc} = 2 \times 10^4$ cells/ml) during the first 3 post-fracture (PF) days [21]. An initial amount of chondrogenic growth factors is assumed at the degrading bone ends ($g_c^{bc} = 2 \times 10^4$ mg/ml) during the first 5 PF days. Osteogenic growth is also delivered through the cortex factors during the first 10 PF days ($g_b^{bc} = 2 \times 10^4$ mg/ml). The initial positions of the tip cells are shown in Fig. 1. Endothelial cells leave the callus domain freely [21].

The periosteal region, which is in close contact with the soft tissues, serves as a source of ultrasound acoustic pressure in order to simulate transducers' application during axial ultrasound transmission. We investigate four different cases of acoustic pressure boundary conditions i.e., $p_1 = 0.8$, $p_2 = 2$, $p_3 = 4$ and $p_4 = 6.1$ kPa (derived from Eq. (17)) which simulate ultrasound application/treatment strategies at different intensities.

Finally, it should be mentioned here that all the bone healing predictions, reported in the present work, have been calculated through the two-dimensional (2D) model shown in Fig. 1. The model of Fig. 1 has been used in order to obtain all the stages of osteogenesis. It is well known that secondary bone healing is a complex procedure taken place in four stages, i.e. the inflammatory, callus differentiation, ossification and bone remodeling stages, all characterized by biochemical signals,

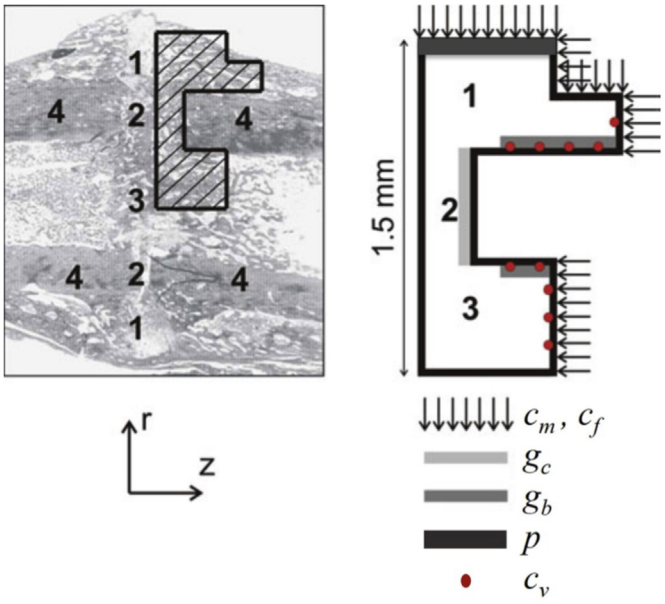

Fig. 1. Model of callus geometry derived from one fourth of real fracture callus geometry at postfracture week 3 [12] due to symmetry [35] (1) periosteal callus; (2) intercortical callus; (3) endosteal callus; (4) cortical bone. Boundary conditions on c_m: mesenchymal stem cells; c_f: fibroblasts; g_c: chondrogenic growth factors; g_b: osteogenic growth factors; c_v: endothelial cells; p: interstitial fluid pressure.

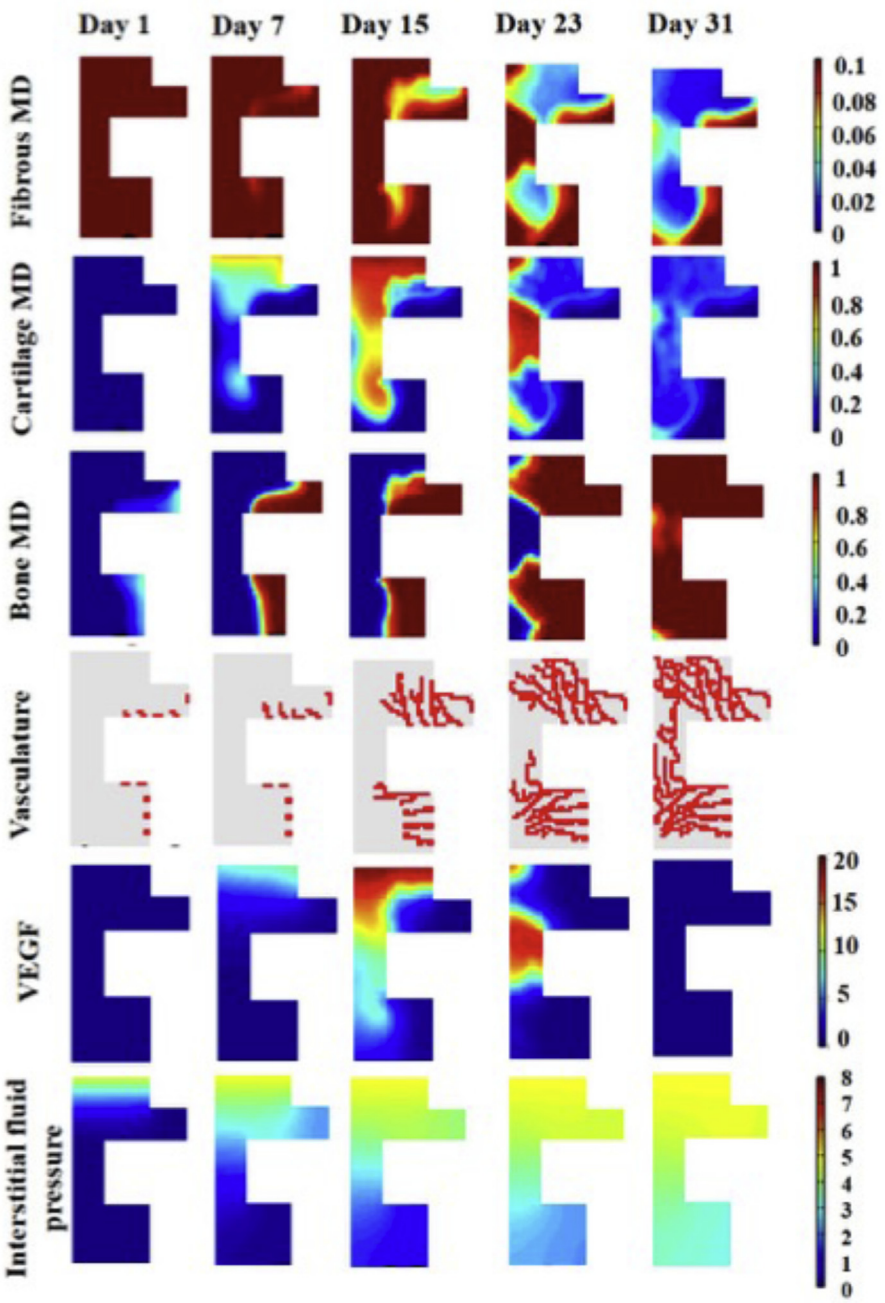

Fig. 2. Predicted spatiotemporal evolution of fibrous tissue, cartilage bone matrix density (MD) (MD, × 0.1 g/ml), vasculature and VEGF (×100 ng/ml) under the presence of Ultrasound ($D_p = 2.35 \times 10^{-3}$) for $K = 0.1$. The spatiotemporal evolution of the interstitial fluid pressure (Pa) of ultrasound is also presented.

mechanical stimuli and plethora of other impressive cellular and molecular processes. Although it seems a rough approximation of the real three-dimensional (3D) problem that simplification is not far from the real bone regeneration process since bone healing is almost an axisymmetric problem.

The system of the partial differential equations is numerically solved with the method of lines (MOL). Spatial discretization of the PDEs is implemented using the finite volume method to ensure mass conservation and non-negativity of the variables [20]. The model is solved on a 2D grid with a grid cell size of 25 μm. The derived ordinary differential equations (ODE) are integrated in time using ROWMAP, a ROW-code of order 4 with Krylov techniques for large stiff ODEs [51]. An extensive convergence analysis, the same applied by Peiffer et al. [35], on the grid cell size and time step size has been performed also in the present work. More details can be found in Peiffer et al., [35].

4. Results

In the present section, numerical simulations based on the above-mentioned numerical implementation are performed for several values of hydraulic conductivity $\widetilde{K}$ and ultrasound intensities I in order to provide insight in the mechanisms that are triggered from ultrasound application during bone healing and investigate the robustness of the proposed model. Evaluation of the ultrasound model is also achieved from comparisons of the predicted spatiotemporal evolution of several tissue fractions in periosteal, intercortical and endosteal callus with data derived by relevant experimental reports [23,30].

The evolution of the tissue density in the callus during normal healing with and without the presence of ultrasound is presented in Figs. 2 and 3 respectively. Fig. 2 presents bone healing predictions for $\widetilde{D}_p = 2.35 \times 10^{-3}$, $\widetilde{K} = 0.1$. Both models can successfully describe the

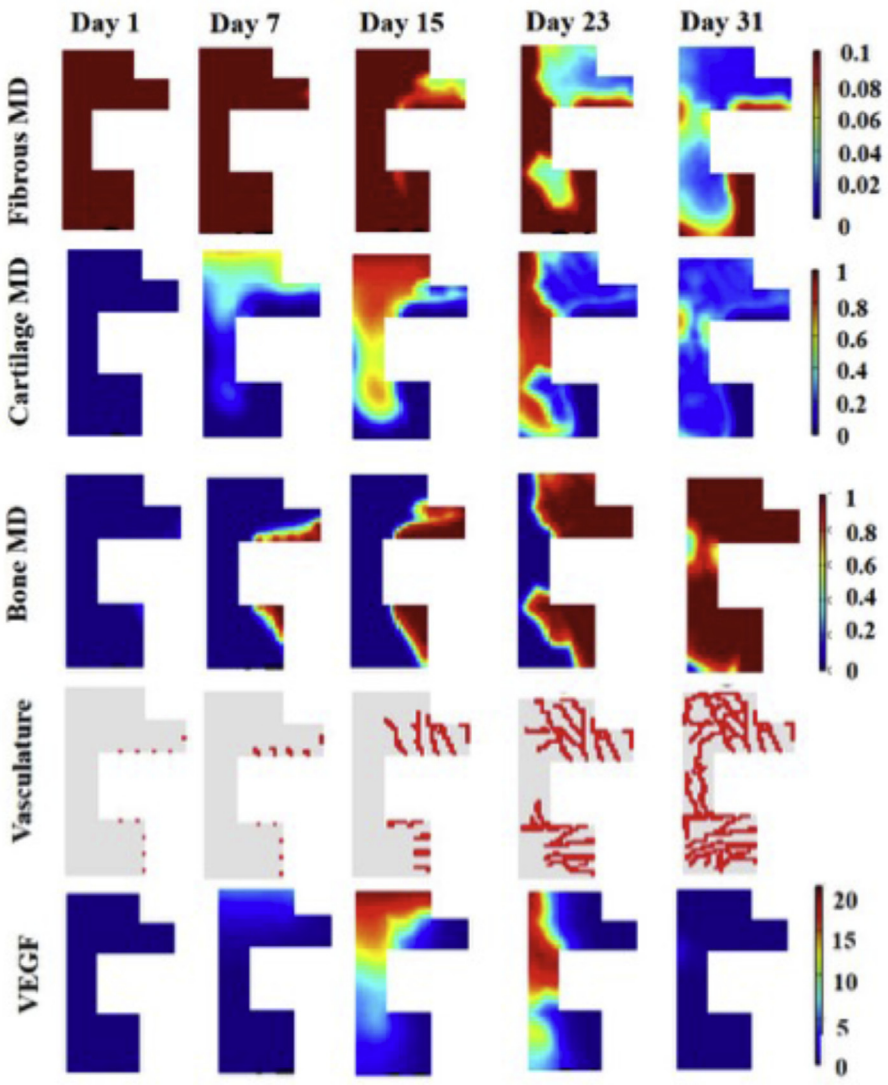

Fig. 3. Predicted spatiotemporal evolution of fibrous tissue, cartilage bone matrix density (MD) (MD × 0.1 g/ml), vasculature and vascular growth factor without the presence of Ultrasound [35].

most important features of bone healing which starts with the migration of mesenchymal cells, fibroblasts and the release of growth factors into the callus from the surrounding tissues. Near the cortex and at a distance from the fracture gap the mesenchymal stem cells differentiate into osteoblasts while in the rest of the callus they differentiate into chondrocytes. When chondrocytes become hypertrophic the angiogenic and osteogenic process starts by producing vascular growth factors. Without the ultrasound effect this occurs at the first post fracture week i.e., PFW 1 in the periosteal callus, which includes the first blood vessels, and at PFW 2 in the endosteal callus (Fig. 3). Under the ultrasound effect angiogenesis starts in the periosteal callus at day 3 PF and in the endosteal at day 8 i.e., about a week earlier than without the ultrasound effect (Fig. 3).

Thereafter the vessels deliver oxygen and nutrients which leads to endochondral ossification. The gap is then gradually filled with bone while the densities of cartilage and fibrous tissue decrease. In Fig. 2 the intercortical ossification starts at around day 23. However, in Fig. 3 i.e., without the ultrasound effect, this occurs 5–6 days later. Meanwhile, blood vessels grow and develop a network that occupies the whole callus region and supplies the complete fracture with oxygen and nutrients. It can be seen that ultrasound leads to enhanced branching and anastomosis creating faster the vascular network within the callus region. In that case bone healing is completed at around day 26 PF. However, without the ultrasound presence bone healing takes around 4–5 weeks.

Fig. 4 presents the blood vessel network for ultrasound intensity $I = 50$ mW/cm^2 and for different values of $\widetilde{K}$ ranging from 0.001 to 0.1. For $\widetilde{K} = 0.001$ and $\widetilde{K} = 0.01$ the tip cells move more or less in similar directions. As $\widetilde{K}$ increases, blood vessels are shown to create more branches and occupy the callus area earlier. More specifically for $\widetilde{K} = 0.1$ branching starts earlier than the other cases. Furthermore, at day 23 the blood vessels have almost fully occupied the endosteal and periosteal callus and have started invading in the intercortical callus.

Fig. 5 presents the evolution of bone matrix density and the vascular density in the callus region for three examined values of $\widetilde{K}$ i.e., $\widetilde{K} = 0.001, 0.01, 0.1$. The corresponding results derived from the model without the ultrasound effect [35] are also depicted in each figure. It can be seen that for $\widetilde{K} = 0.1$ the bone matrix density takes higher values throughout the whole healing course than for the other examined values as well as for the model without the ultrasound effect (Fig. 5(a)). More specifically in the control model (i.e., without the ultrasound application) at day 25 PF the bone matrix is equal to 69.77% whereas under the ultrasound presence, for $\widetilde{K} = 0.1$, it is equal to 84.22%. For $\widetilde{K} = 0.01$ bone matrix density is almost identical to that for $\widetilde{K} = 0.001$

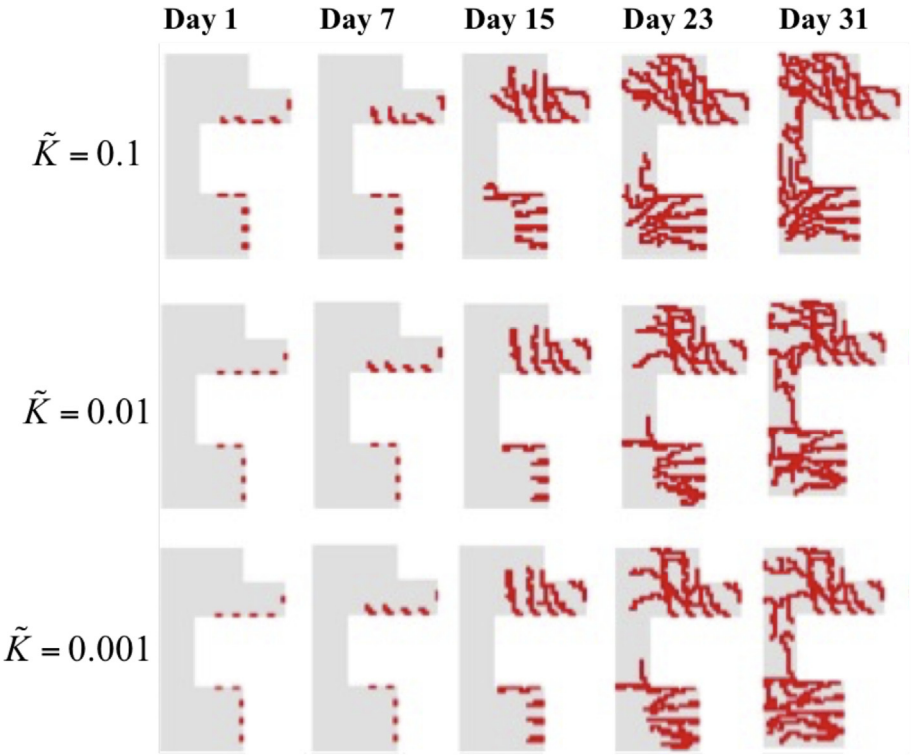

Fig. 4. The evolution of vasculature for different values $\tilde{K}$ ranging from 0.001 to 0.1. In this case the ultrasound intensity equals to $I = 50\,\mathrm{mW/cm^2}$.

and takes higher than the case without ultrasound until day 23 PF. Thereafter it becomes slightly lower which indicates a more pronounced effect of ultrasound in the onset of the healing process. Similar observations can also be made for the vascular densities in the callus Fig. 5(b), with the optimal case, by means of blood vessel density, to be for $\tilde{K} = 0.1$. At day 30 PF the vascular density in the initial model equals to 36.64% whereas in the ultrasound model for $\tilde{K} = 0.1$ equals to 40.47%, respectively. Regarding the cases for the lower examined values of $\tilde{K}$, the vascular density exhibits a similar behavior until day 22, taking greater values than the case without ultrasound. Thereafter for $\tilde{K} = 0.01$ it increases more rapidly reaching higher amounts than the initial model. However, for $\tilde{K} = 0.001$ the vascular density is slightly lower (until day 28) or the same (at day 30) as the model without ultrasound. Similar analysis for other parameters can be also performed but the two chosen here are of outmost interest for the purpose of this study.

Table 1 presents the surface fraction of blood vessels in the callus throughout the healing course derived from the ultrasound model ($\tilde{K} = 0.1$) as well as from the model without ultrasound. Augmented fractions are found for the ultrasound model with the deviation to be stronger for PFW2 and PFW3.

As Betts and Muller [3] mention, the comparison between predictions provided by simulations and experimental studies remains an obstacle for advancing the field. However, Fig. 6 compares the experimentally determined temporal evolution of the tissue fractions in the periosteal, intercortical and endosteal callus [22], with the predictions of the Peiffer model [35] and the results from the proposed ultrasound model (for$\tilde{K} = 0.1$). In order to calculate the tissue fractions, the spatial images are first binarised employing tissue-specific thresholds (0 when the tissue does not exist and 1 when the tissue exists in a grid cell). Then, an equal weight is assigned to the different tissues, i.e. if three tissues are contained in a grid cell, that specific grid cell area is divided by three when the tissue fractions are calculated. It can be seen that both models are able to predict the general trends in the experimental data [23] i.e., the bone fraction gradually increases as the fibrous tissue disappears and the cartilage first rises, reaches a peak and then declines. However, all processes of tissue formation and degradation in the whole callus area are affected by US presence. The fibrous tissue decreases with a higher rate in the periosteal and endosteal callus than the model without ultrasound. Furthermore, the experimentally measured cartilage amounts in the endosteal callus are also higher than those predicted from the ultrasound model during healing. At days 5 and 23 the fibrous tissue fraction in the endosteal callus is 72.67% and 2% respectively in the ultrasound model as compared with 94.17% (day 5) and 10% (day 23) in the model without ultrasound. Meanwhile the experimental data [23] indicate such as in the case of cartilage higher amounts of fibrous tissue fraction compared to the ultrasound model. In more detail, it can be seen 80% fibrous tissue fraction at day 5 and 42% at day 20. In addition under the influence of ultrasound cartilage formation in the endosteal callus starts at day 9 i.e., 4 days earlier than without ultrasound and is completed at day 25, i.e., 5 days later. Finally, the bone tissue fraction is predicted to increase faster in the ultrasound model with the differences to be more significant in the endosteal callus. More specifically in the endosteal, callus bone fraction increases from 60.83% (day 20) in the ultrasound model (vs. 28.44% in the model without ultrasound and 55% observed experimentally by Harrison et al. [23]) to 91.98% (day 30) (vs. 86% without ultrasound and 74% observed experimentally by Harrison et al. [23]). In the periosteal callus bone fraction increases from 42.58% (day 15) in the ultrasound model (vs. 30.42% in the model without ultrasound) to 93.75% (day 25) (vs. 85.42% without ultrasound).

Development of blood vessel network for different ultrasound intensities ranging from 15 to 75 $\mathrm{mW/cm^2}$ is illustrated in Fig. 7. It can be seen that in all cases (either with or without US) in the first PFW the vasculature is limited and only away from the fracture line a few blood vessels are present. Nevertheless, after day 14 PF, under the ultrasound effect and for all the examined ultrasound intensities blood vessels in the periosteal and endosteal callus seem to grow and create branches more rapidly than in the initial model. Furthermore, in all cases ultrasound steers the tips in more or less similar directions different from those observed in the model of Peiffer et al., [35]. Ultrasound speeds up angiogenesis with the effect to be more pronounced as the intensity

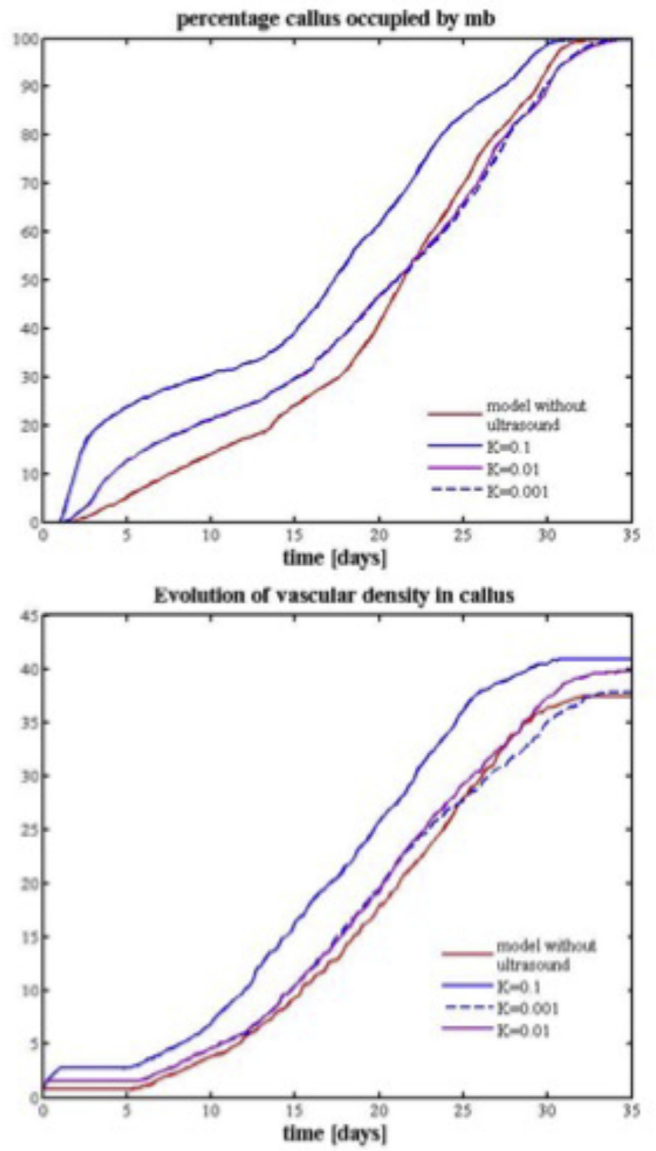

Fig. 5. Predicted temporal evolution of bone matrix density and vascular density in callus for different $K = 0.1$, $K = 0.01$ and $K = 0.001$. The corresponding results for the model without the ultrasound effect i.e. the model of [35] are also presented.

Table 1
Surface fractions of blood vessels in callus (%).

	PFW2 (DAY 14)	PFW3 (DAY 21)	PFW4 (DAY 28)
$\widetilde{K} = 0.1$	14.06	27.42	39.38
Model without US	8.05	19.53	33.91

increases up to 50 mW/cm^2. However, a further increase of the intensity (i.e., for $I = 75$ mW/cm^2) does not have any positive impact. As opposed to the initial model the blood vessels under the ultrasound effect for $I = 50$ mW/cm^2 have almost fully occupied the callus at day 23 apart from a small region in the endosteum. Given that at this day the corresponding bone matrix density in the callus is 90.39% (Fig. 7) the vasculature contributed enhanced bone formation, resulting in a clinical union. The results render the value of 50 mW/cm^2 as the optimal intensity that leads to accelerated angiogenic process.

Fig. 8 presents the percentages of callus area covered with bone observed experimentally by Miedel et al. [30], at days 10 and 20 post fracture also reported in OReilly et al. [33], along with the corresponding values predicted from the ultrasound model and the model of Peiffer et al., [35]. It can be seen that the model of Peiffer et al. [35], predicts similar percentages of bone in the callus region with the experimental data i.e., less than 10% at day 10 and 40% at day 20. These values are found significantly increased under the presence of ultrasound i.e., 30% at day 10 and 60% at day 20.

5. Discussion

In this work we presented for the first time a hybrid mathematical model for deriving bone healing predictions under the effect of ultrasound. Since the exact mechanisms by which ultrasound accelerates bone healing are unknown the aim of this model was to provide novel insights and fundamental understanding of the influence of ultrasound on bone regeneration and angiogenesis. The model was based on the one described in Peiffer et al. [35], and was further extended by i) including an additional equation describing the spatiotemporal evolution of the acoustic interstitial fluid pressure and ii) appropriately modifying the equation that describes the spatiotemporal evolution of VEGF. Ultrasound was assumed to primarily affect VEGF transport, which is in accordance with previous in vitro studies on human cells [12,42]. Ultrasound affects other factors as well but we have limited this work only to VEGF. In a future communication this will be extended to other factors.

The diffusivity of the acoustic pressure D_p was calculated by using the material properties of granulation tissue, which occupies the whole callus region at the onset of the healing process. In this respect the hydraulic conductivity $\widetilde{K}$ was also firstly assumed equal to the permeability coefficient of the granulation tissue i.e., $\widetilde{K} = 0.1$. However, in order to corroborate this assumption and investigate the sensitivity of the model's outcome simulations were also performed by assuming values which correspond to dimensionalized permeability coefficients of all the tissues involved in bone healing process [12]. It should be also noted that values that fall out of the examined range lead to either no blood vessel formation or physically unacceptable results and were thus deliberately ignored here.

In all the examined cases the model was able to capture significant events of the normal fracture healing process such as intramembranous and endochondral ossification. However, under the US effect and for $\widetilde{K} = 0.1$ the ossification process was found to be accelerated (by around 10 days), which is attributed to the positive influence on the angiogenesis mechanisms. More specifically ultrasound leads to i) an earlier onset of angiogenesis in the periosteal and endosteal callus ii) enhanced branching mechanisms and iii) accelerated development of blood vessel network throughout the whole callus region.

The sensitivity analysis for $\widetilde{K}$ shows that ultrasound steers the tip cells in similar directions that differ from those in the initial model [35]. This is imposed by the additional boundary condition of ultrasound acoustic pressure at the periosteal callus. In all the examined cases, after the second PF week, branching was enhanced leading thus to the development of more dense blood vessel network as compared with the case without US. The most significant effect was observed for the highest value ($\widetilde{K} = 0.1$) i.e., when VEGF transport is highly affected by the US acoustic pressure. Reduced $\widetilde{K}$ values i.e., $\widetilde{K} = 0.1$, 0.01 cause a delayed invasion of the tip cells in the endosteal callus which is reasonable since K is related to the ability of US to pass through the callus area. Calculation of the temporal evolution of bone matrix and vascular densities in the callus region throughout the healing course also showed higher values for $\widetilde{K} = 0.1$, rendering thus 0.1 as the most optimal value. More specifically higher amounts of blood vessels were observed in the ultrasound model ($\widetilde{K} = 0.1$) with the deviation to be more pronounced at weeks 2–4. Increased blood vessel formation due to ultrasound has also been reported in various animal fractures using techniques such as Doppler assessment [9,29].

Comparisons of the volume fractions of all tissues in the endosteal,

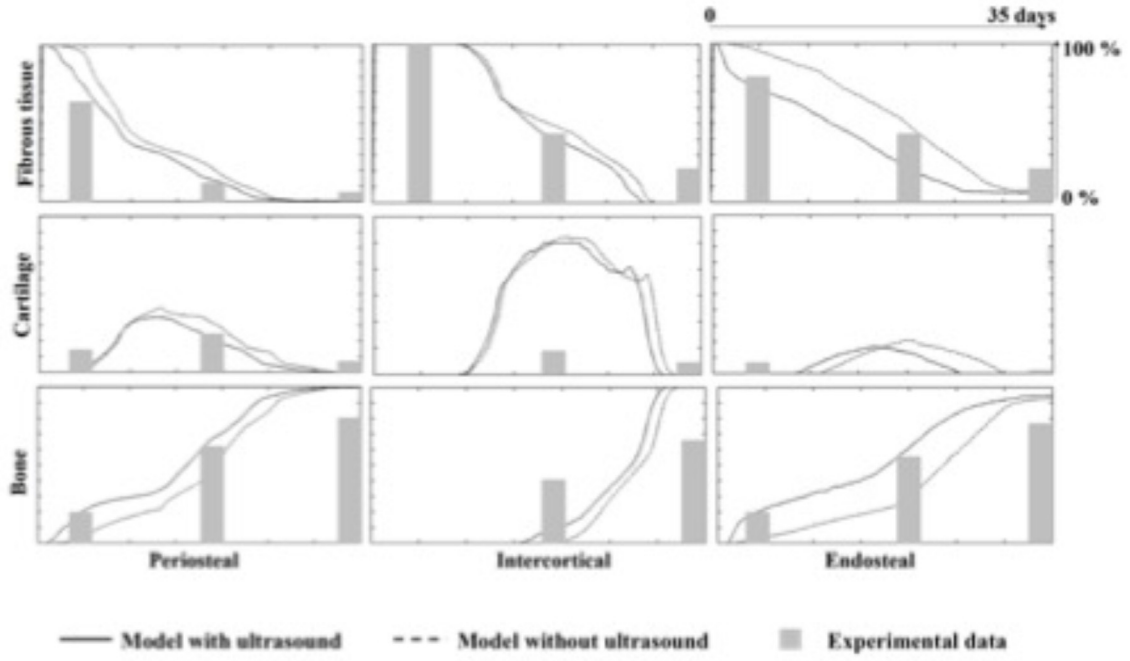

Fig. 6. Prediction of the temporal evolution of the bone cartilage and fibrous tissue fractions (%) in the periosteal, intercortical and endosteal callus derived from the newly developed model with ultrasound for $K = 0.1$ and the model without ultrasound [35].

periosteal and intercortical callus during the healing course among the computational models and experimental measurements [23] showed that both computational models can capture effectively the spatio-temporal dynamics of bone healing process. However, both computational models predict a faster resorption of fibrous tissue matrix than that observed experimentally. In addition, the healing process predicted by both models evolves faster than what is experimentally observed by Harrison et al., [23]. A first explanation for that is the use of 2D instead of 3D model geometry. Also, as it has been already discussed in Peiffer et al. [35], this could be attributed to the fact that the maturation of the time cells is not accounted in the hybrid model. Furthermore, although the trend of the cartilage evolution predicted from both models is in agreement with the experimental data [23], the predicted cartilage density values were unnaturally increased. According to Peiffer et al. [35], this could be due to the fact that the hybrid model does not account for the oxygen and nutrients to the cartilage production process. However this overestimation of the amount of cartilage matrix was also found in two more recent studies of [5,6] which constitute extensions of the Peiffer model [35] by incorporating a detailed description of the impact of oxygen on the cellular processes during bone healing and was attributed to the fact that progenitor cells are assumed to differentiate towards both the chondrogenic and osteogenic lineage which does not occur in reality [5].

An in-depth comparison between the proposed and the initial models reveals some differences that are indicative of the ultrasound influence. In the ultrasound model: i) the cartilage fraction in the periosteal callus decreases faster and ii) in the endosteal callus cartilage formation and degradation occurs earlier than in the model without the ultrasound effect (Fig. 6). Although these findings constitute downstream effects since they have not explicitly modeled herein, they may be indicative of an earlier endochondral ossification and are consistent with several in vitro and *in vivo* studies reporting that US leads to earlier chondrogenesis and cartilage hypertrophy causing earlier endochondral ossification [29]. In this respect a possible US affected pathway that could be suggested from the proposed model (i.e., by accounting a direct US influence on the VEGF transport) may be that of the endochondral ossification [29].

Furthermore, the ultrasound model derives a more rapid decrease in the fibrous tissue volume fraction and an increased bone formation rate than both the model of Peiffer et al. [35], and the experimental measurements, leading thus to higher bone matrix levels and accelerated healing time. This result was further supported from comparisons between the predictions derived from both models with additional in-vivo measurements [30] from murine osteotomies. Interestingly the model of Peiffer et al. [35], predicted almost equal bone matrix percentages in the callus region at days 10 and 20 post fracture. However, the proposed model yielded 20% higher bone formation within the callus region, demonstrating the enhancement role of ultrasound. Our findings are also in agreement with other previous animal studies on a sheep osteotomy which report that transosseous ultrasound application leads to an increase in bone matrix density and a speed up in healing time [38]. Increased levels of bone density due to ultrasound are also reported in Refs. [17,50].

Since ultrasonic parameters have been experimentally shown to influence the effect of US on angiogenesis and bone healing mechanisms, numerical simulations were also performed herein for different intensity values, which (by using Eq. (17)) correspond to different boundary conditions of acoustic pressure. The examined range of intensities (i.e., 15–75 mW/cm^2) is typically used in experimental studies using Low Intensity Ultrasound [40,54]. For the first two PFW, US was found to enhance the evolution of vasculature with the influence to be more significant as the intensity increases. Nevertheless, this is not the case after the reparative phase since for the highest intensity i.e., $I = 75\ mW/cm^2$ the US effect on blood vessel network decreases. Our results suggest that ultrasound application at $I = 50\ mW/cm^2$ has the greatest effect on angiogenic and bone healing processes and could be thus regarded as an optimal value to be used in ultrasound treatment regimens. This finding comes in agreement with a previous animal study [54] which report that femoral fractures treated at $50\ mW/cm^2$ exhibited higher torsional stiffness and maximum torque than those treated at $100\ mW/cm^2$.

The remodeling phase of bone healing is not addressed by the proposed model. Nevertheless, the direct effects of US on the cellular processes involved in the bone remodeling stage of healing have not been elucidated yet. In Ref. [32] the authors suggest the hemodynamic shear stress caused by the LIPUS-induced increase in blood pressure as

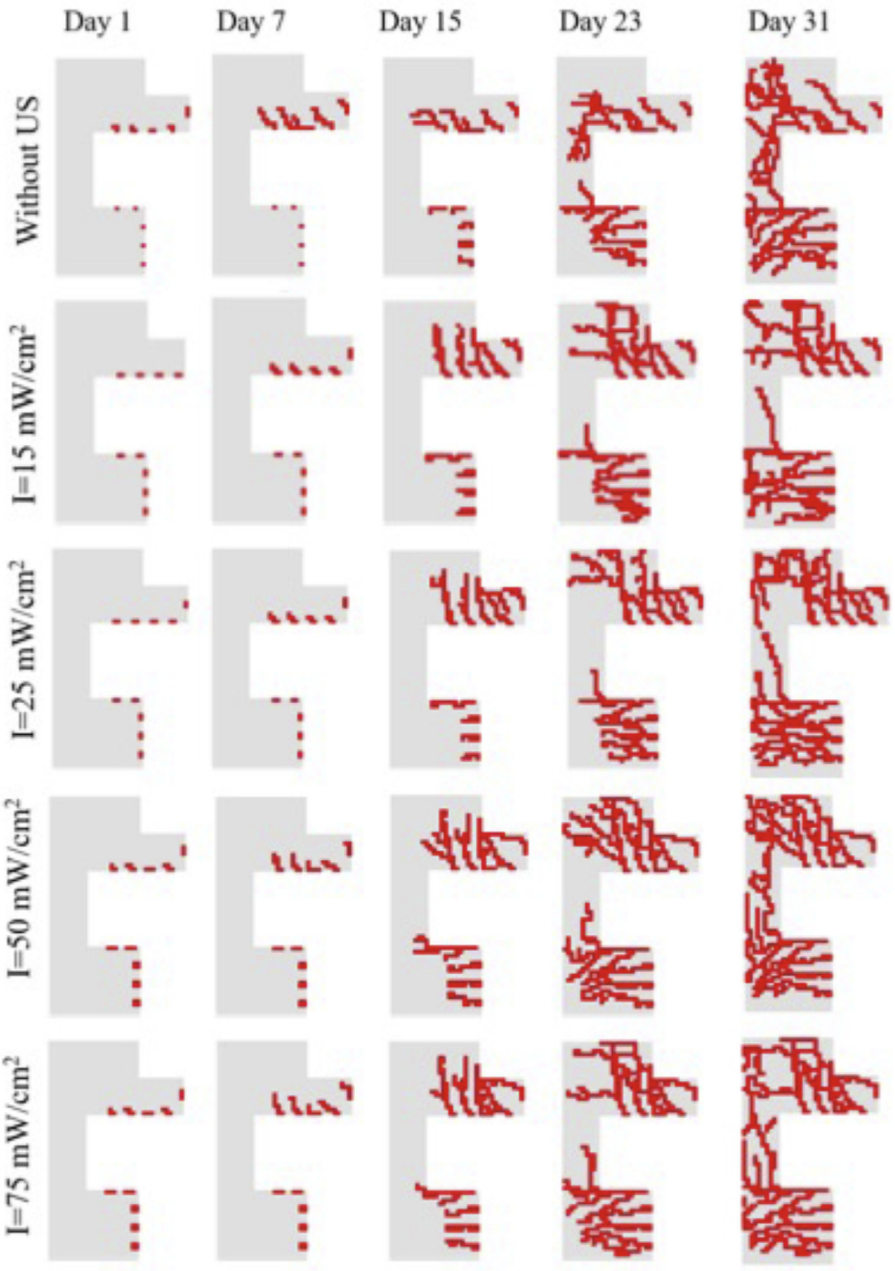

Fig. 7. The evolution of vasculature for different ultrasound intensities i.e., $I = 15, 25, 50, 75$ mW/cm^2. In this case $K = 0.1$. The corresponding results for the model without the ultrasound effect, i.e. the model of [35] are also presented.

well as the subsequent increased fluid flow and fluid turbulence at the fracture site to play significant role in bone remodeling by causing the gathering of osteoprogenitor cells from the marrow.

A further limitation of our study is that the effect of the mechanical environment on the regeneration process are not taken into account. However, variations in the stability of the fracture and the motion between the bone fragments are known to influence cellular processes such as cell migration, proliferation and differentiation as well as matrix formation and angiogenesis [36]. However, the effect of mechanical loading may be more pronounced in models of large animals, which is not the case of the present study. Nevertheless, the adaptation of the ultrasound model so as to also incorporate the impact of the callus mechanical environment would provide significant information and constitute a valuable extension of the proposed framework.

It should be also remarked that the callus is modeled in this study as a simple 2D model neglecting its complex three-dimensional geometry. Two-dimensional models have been widely used for the study of ultrasound propagation during bone healing [38]. In addition, under specific circumstances i.e., when the ratio of the wall thickness to the outer radius is small, the theory predicts that ultrasound dispersion in tube can be practically approximated by the corresponding modes in a plate [48]. Furthermore, as also stated in Peiffer et al. [35], the use of lower-dimensional models as a first approach of a study constitutes a well-established method in applied mathematics since geometric complexity and computational costs render the investigation of 3D models much more complicated [43].

As previously mentioned ultrasound has been experimentally found to affect multiple cellular mechanisms during bone healing. In this respect we have extended by performing some initial simulations that also account for the effect of ultrasound on osteoblasts proliferation and VEGF production. Nevertheless, further investigation is needed in order to draw safe conclusions and determine whether certain scenarios of US

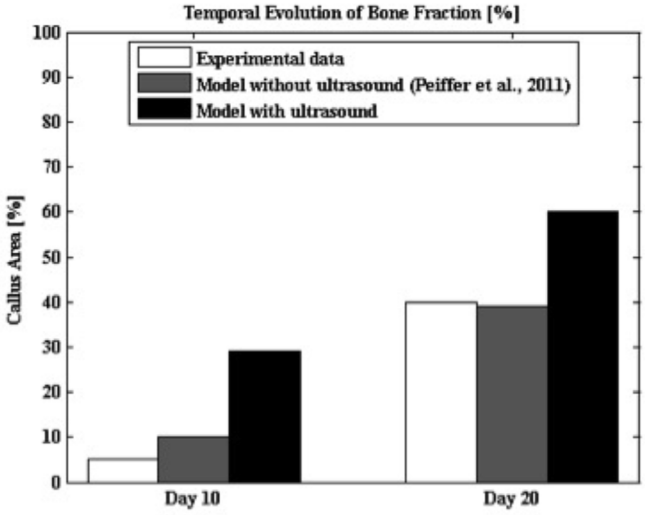

Fig. 8. Percentages of bone observed experimentally by Miedel et al. [30], (those do not take into account the presence of US), derived from model's simulation without ultrasound [35] and with ultrasound at PF day 10 and 20.

affected mechanisms are more plausible than others.

6. Conclusions

In this work we present for the first time a bioregulatory model that accounts for the effect of ultrasound on angiogenesis and bone healing mechanisms. Ultrasound was modeled to primarily affect VEGF transport by i) inserting two additional parameters in the mathematical framework (i.e., D_p and K) and ii) applying an additional boundary condition of ultrasound acoustic pressure at the periosteal region of callus, which simulates the presence of US transducer during axial transmission. It was found that ultrasound plays key role in angiogenesis and leads to accelerated completion of blood vessel network. The influence was more pronounced for $\widetilde{K} = 0.1$ i.e., for the highest examined value of hydraulic conductivity. Furthermore, investigation of the effect of ultrasound intensity showed that the greatest effect on angiogenic and bone healing processes was achieved for $I = 50\,\mathrm{mW/cm^2}$, which is suggested as an optimal value to be used in ultrasound treatments. By comparing with experimental measurements of normal bone healing [23,30] it was demonstrated that ultrasound enhances the endochondral ossification process accelerating bone formation and reduces significantly the healing course given that it is observed a much more rapid decrease in the fibrous tissue volume fraction. Mathematical models accounting for the multifaceted effect of ultrasound could be regarded as a useful tool for the orthopedic surgeons assisting them to predict the treatment outcome, early diagnose complications and continuously monitor the progress of healing course.

Acknowledgments

The research project is implemented within the framework of the Action «Supporting Postdoctoral Researchers» of the Operational Program "Education and Lifelong Learning" (Action's Beneficiary: General Secretariat for Research and Technology), and is co-financed by the European Social Fund (ESF) and the Greek State (PE8-3347).

Aurélie Carlier is a post-doctoral fellow of the Research Foundation Flanders (FWO-Vlaanderen).

References

[1] D. Anderson, P. Thaddeus, A. Marin, J. Elkins, W. Lack, D. Lacroix, Computational techniques for the assessment of fracture repair, Injury, Int. J. Care Injured 45S (2014) S23–S31.
[3] D. Betts, R. Muller, Mechanical regulation of bone regeneration: theories, models, and experiments, Front. Endocrinol. 5 (2014) 211.
[4] R.A.D. Carano, E.H. Filvaroff, Angiogenesis and bone repair, Drug Discov. Today 8 (21) (2003) 980–989.
[5] A. Carlier, L. Geris, N.V. Gastel, G. Carmeliet, H.V. Oosterwyck, Oxygen as a critical determinant of bone fracture healing: a multiscale model, J. Theor. Biol. 365 (2015) 247–264.
[6] A. Carlier, L. Geris, K. Bentley, G. Carmeliet, P.V. Carmeliet, MOSAIC: a multiscale model of osteogenesis and sprouting angiogenesis with lateral inhibition of endothelial cells, PLoS Comput. Biol. 8 (2012) e1002724.
[7] S. Checa, P.J. Prendergast, A mechanobiological model for tissue differentiation that includes angiogenesis: a lattice-based modeling approach, Ann. Biomed. Eng. 37 (1) (2009) 129–145.
[8] W.H. Cheung, K.S. Leung, S.K.H. Chow, Ultrasound and fragility fracture: is there a role? Injury, Int. J. Care Injured 47 S1 (2016) S39–S42.
[9] W.H. Cheung, S.K. Chow, M.H. Sun, Qin Ling, Kwok-Sui Leung, Low-intensity pulsed ultrasound accelerated callus formation, angiogenesis and callus remodeling in osteoporotic fracture healing, Ultrasound Med. Biol. 37 (2) (2011) 231–238.
[10] S.K. Chow, K.S. Leung, L. Qin, F. Wei, W.H. Cheung, Callus formation is related to the expression ratios of estrogen receptors-alpha and -beta in ovariectomy- induced osteoporotic fracture healing, Arch. Orthop. Trauma Surg. 134 (2014) 1405–1416.
[11] L. Claes, B. Willie, The enhancement of bone regeneration by ultrasound, Prog. Biophys. Mol. Biol. 93 (2008) 384–398.
[12] S.C. Cowin, Bone poroelasticity, J. Biomech. 32 (1999) 217–238.
[13] N. Doan, P. Reher, S. Meghji, M. Harris, In vitro effects of therapeutic ultrasound on cell proliferation, protein synthesis and cytokine production by human fibroblasts, osteoblasts, and monocytes, J. Oral Maxillofac. Surg. 57 (1999) 409–419.
[14] L.R. Duarte, The stimulation of bone growth by ultrasound, Arch. Orthop. Trauma Surg. 101 (1983) 153–159.
[15] O. Erdogan, E. Esen, Biological aspects and clinical importance of ultrasound therapy in bone healing, J. Ultrasound Med. 28 (6) (2009) 765–776.
[16] C.H. Fung, W.H. Cheung, N.M. Pounder, A. Harrison, K.S. Leung, Osteocytes exposed to far field of therapeutic ultrasound promotes osteogenic cellular activities in pre-osteoblasts through soluble factors, Ultrasonics 54 (2014) 1358–1365.
[17] C.H. Fung, W.H. Cheung, N.M. Pounder, A. Harrison, K.S. Leung, Effects of different therapeutic ultrasound intensities on fracture healing in rats, Ultrasound Med. Biol. 38 (5) (2012) 745–752.
[18] L. Geris, A. Gerisch, R. Schugart, Mathematical modeling in wound healing, bone regeneration and tissue engineering, Acta Biotheor. 58 (2010) 355–367.
[19] L. Geris, A. Gerisch, J. Vander Sloten, R. Weiner, H. Van Oosterwyck, Angiogenesis in bone fracture healing: a bioregulatory model, J. Theor. Biol. 25 (2008) 137–158.
[20] A. Gerisch, M.A.J. Chaplain, Robust numerical methods for taxis-diffusion-reaction systems: applications to biomedical problems, Math. Comput. Model. 43 (2006) 49–75.
[21] L. Gerstenfeld, D. Cullinane, G. Barnes, D. Graves, T. Einhorn, Fracture healing as a post-natal developmental process: molecular, spatial, and temporal aspects of its regulation, J. Cell. Biochem. 88 (5) (2003) 873–884.
[22] M.S. Ghiasi, J. Chen, A. Vaziri, E.K. Rodriguez, A. Nazarian, Bone fracture healing in mechanobiological modeling: a review of principles and methods, BoneKEy Rep. 6 (2017) 87–100.
[23] L.J. Harrison, J.L. Cunningham, L. Stromberg, A.E. Goodship, Controlled induction of a pseudarthrosis: a study using a rodent model, J. Orthop. Trauma 17 (2003) 11–21.
[24] J.D. Heckman, J.P. Ryaby, J. McCabe, J.J. Frey, R.F. Kilcoyne, Acceleration of tibial fracture-healing by non-invasive, low-intensity pulsed ultrasound, J Bone Joint Surg Am. 76 (1994) 26–34.
[25] S. Jingushi, M.E. Joyce, M.E. Bolander, Genetic expression of extracellular matrix proteins correlates with histologic changes during fracture repair, J. Bone Miner. Res. 7 (1992) 1045–1055.
[26] M.W. Johnson, Behavior of fluid in stressed bone and cellular stimulation, Calcif. Tissue Int. 36 (Suppl 1) (1984) 72–76.
[27] T.K. Kristiansen, J.P. Ryaby, J. McCabe, J.J. Frey, L.R. Roe, Accelerated healing of distal radial fractures with the use of specific, low-intensity ultrasound. A multicenter, prospective, randomized, double blind, placebo-controlled study, J Bone Joint Surg Am. 79 (1997) 961–973.
[28] J. Kusuyama, K. Bandow, M. Shamoto, K. Kakimoto, T. Ohnishi, T. Matsuguchi, Low-intensity pulsed ultrasound (LIPUS) influences the multi-lineage differentiation of mesenchymal stem and progenitor cell lines through ROCK-Cot/Tpl2-MEK-ERK signaling pathway, J. Biol. Chem. 289 (2014) 10330–10344.
[29] P. Martinez de Albornoz, A. Khanna, U.G. Longo, F. Forriol, N. Maffulli, The evidence of low-intensity pulsed ultrasound for in vitro, animal and human fracture healing, Br. Med. Bull. 100 (1) (2011) 39.
[30] E. Miedel, M.I. Dishowitz, M.H. Myers, D. Dopkin, Y.Y. Yu, T.S. Miclau, R. Marcucio, J. Ahn, K.D. Hankenson, Disruption of thrombospondin-2 accelerates ischemic fracture healing, J. Orthop. Res. 31 (6) (2013) 935–943.
[31] F. Milde, M. Bergdorf, P. Koumoutsakos, A hybrid model for three-dimensional simulations of sprouting angiogenesis, Biophys. J. 95 (2008) 3146–3160.
[32] R. Mundi, S. Petis, R. Kaloty, V. Shetty, M. Bhandari, Low-intensity pulsed ultrasound: fracture healing, Indian J. Orthop. 43 (2) (2009) 132–140.
[33] A. OReilly, K.D. Hankenson, D.J. Kelly, A computational model to explore the role of angiogenic impairment on endochondral ossification during fracture healing, Biomechanics Model. Mechanobiol. (2016) 1–16.
[34] F. Padilla, R. Puts, L. Vico, K. Raum, Stimulation of bone repair with ultrasound: a review of the possible mechanic effects, Ultrasonics 54 (2014) 1125–1145.
[35] V. Peiffer, A. Gerisch, D. Vandepitte, O.H. Van, L. Geris, A hybrid bioregulatory

model of angiogenesis during bone fracture healing, Biomechanics Model. Mechanobiol. 10 (2011) 383–395.
[36] S. Perren, J. Cordey, The concept of interfragmentary strain, in: H.K. Uhthoff (Ed.), Current Concepts of Internal Fixation of Fractures, Springer, Berlin, 1980, pp. 63–77.
[37] C. Phipps, M. Kohandel, Mathematical model of the effect of interstitial fluid pressure on angiogenic behavior in solid tumors, Comp. and Math. Meth in Med (2011) 1–9.
[38] V. Protopappas, M. Vavva, D. Fotiadis, K. Malizos, Ultrasonic monitoring of bone fracture healing, IEEE Trans. Ultras., Ferroel., and freq. cont 55 (2008) 1243–1255.
[39] A. Qutub, A. Popel, Elongation, proliferation & migration differentiate endothelial cell phenotypes and determine capillary sprouting, BMC Syst. Biol. 3 (13) (2009) 1–24.
[40] R. Ramli, P. Reher, M. Harris, S. Meghji, The effect of ultrasound on angiogenesis: an in vivo study using the chick chorioallantoic membrane, Int. J. Oral Maxillofac. Implants 24 (4) (2009) 591–596.
[41] N.M. Rawool, B.B. Goldberg, F. Forsberg, A.A. Winder, E. Hume, Power Doppler assessment of vascular changes during fracture treatment with low-intensity ultrasound, J. Ultrasound Med. 22 (2003) 145–153.
[42] P. Reher, N. Doan, B. Bradnock, S. Meghji, M. Harris, Effect of ultrasound on the production of IL-8, basic FGF and VEGF, Cytokine 11 (1999) 416–423.
[43] M. Ryser, N. Nigam, S. Komarova, Mathematical modeling of spatiotemporal dynamics of a single bone multicellular unit, J. Bone Miner. Res. 24 (5) (2009) 860–870.
[44] S.J. Shefelbine, P. Augat, L. Claes, U. Simon, Trabecular bone fracture healing simulation with finite element analysis and fuzzy logic, J. Biomech. 38 (2005) 2440–2450.
[45] J. Street, M. Bao, L. deGuzman, S. Bunting, F.V. Peale, N. Ferrara, H. Steinmetz, J. Hoeffel, J.L. Cleland, A. Daugherty, N. van Bruggen, H.P. Redmond, R.A.D. Carano, E.H. Filvaroff, Vascular endothelial growth factor stimulates bone repair by promoting angiogenesis and bone turnover, P. Natl Acad. Sci. USA 99 (15) (2002) 9656–9661.
[46] S. Sun, M. Wheeler, M. Obeyesekere, C.J. Patrick, A deterministic model of growth factor-induced angiogenesis, Bull. Math. Biol. 67 (2005) 313–337.
[47] G.J. Tortora, S.R. Grabowski, Principles of Anatomy and Physiology, tenth ed., John Wiley and Sons, Inc, Hoboken (NJ), 2003.
[48] M.G. Vavva, V.C. Protopappas, L.N. Gergidis, A. Charalambopoulos, D.I. Fotiadis, D. Polyzos, Velocity dispersion of guided waves propagating in a free gradient elastic plate: application to cortical bone, J. Acoust. Soc. Am. 125 (5) (2009) 3414–3427.
[49] M. Wang, N. Yang, X. Wang, A review of computational models of bone fracture healing, Med. Biol. Eng. Comput. 55 (2017) 1895–1914.
[50] S. Warden, J. Favaloro, K. Bennell, J. McMeeken, K. Ng, J. Zajac, J. Wark, Low-intensity pulsed ultrasound stimulates a bone-forming response in UMR-106 cells, Biochem. Biophys. Res. Commun. 286 (3) (2001) 443–450.
[51] R. Weiner, B.A. Schmitt, H. Podhaisky, ROWMAP- a ROW-code with Krylov techniques for large stiff ODEs, Appl. Numer. Math. 25 (1997) 303–319.
[52] S. Wu, Y. Kawahara, T. Manabe, K. Ogawa, M. Matsumoto, A. Sasaki, Low intensity pulsed ultrasound accelerates osteoblast differentiation and promotes bone formation in an osteoporosis rat model, Pathobiology 76 (2009) 99–107.
[53] C. Xu, J.M. Harris, Y. Quan, Estimating flow properties of Porous media with a model for dynamic diffusion, Geoph. Dep. New Orleans, Annual Meeting, 2006, pp. 1831–1835.
[54] K.H. Yang, J. Parvizi, S.J. Wang, Exposure to low-intensity ultrasound increases aggrecan gene expression in a rat femur fracture model, J. Orthop. Res. 14 (5) (1996) 802–9.